Feasibility of Prosthetic Posture Sensing Via Injectable Electronic Modules

Wei Tan, *Member, IEEE*, and Gerald E. Loeb, *Member, IEEE*

***Abstract*—A bionic neuron (BION) is an inductively powered, miniature implant developed for functional electric stimulation (FES) to reanimate paralyzed limbs. This paper investigates the possibility of reusing the BION antenna coil as a magnetic sensor to provide meaningful posture information for feedback control of FES. A variety of techniques have been developed to model and cancel nonideal effects caused by the shapes of the internal and external coils, ferrite material, and electronic connections. Field warping has been employed to both amplitude and direction to achieve more accurate description of the dipole magnetic field generated by external coils suitable for generating a reference magnetic frame in the environment of a wheelchair. Models of the transmitting coil and the receiving BION coil were validated against experimental data, providing a solid foundation for implementing a sensor system. Based on the established model, a magnetic sensing system combined with customized microelectro-mechanical systems (MEMS) accelerometer has been designed and tested as a prototype on the bench. The sensor output can be employed to compute 6-D position and orientation. A two-step algorithm integrated with multiple error-cancelling techniques demonstrated sufficient accuracy in bench tests to appear promising for control of reach-and-grasp tasks. A sensor fusion step is proposed to estimate the position and orientation of a limb segment using data from multiple implants in muscles, where they will also function as neuromuscular stimulators to produce the movements to be controlled.**

***Index Terms*—Bionic neuron (BION), functional neuromuscular stimulation, implantable sensor, magnetic sensors, posture sensing.**

I. Introduction

FUNCTIONAL electrical stimulation (FES) of paralyzed muscles has traditionally focused on getting muscles to produce the requisite torques required for limb movement. Microimplants called BIONs (BIOnic neurons) [1] have been developed to interface with the multiple muscles required for most tasks. They are modularly designed wireless capsules that can be injected into the human body without requiring surgery. Separately addressable BIONs can be implanted at various sites in the body near motor nerves, where they receive power and digital command data from an external radio frequency (RF) coil and deliver stimulating current pulses to recruit the motor neurons and activate associated muscles. Given appropriate control strategies, this technology could be used create useful movement in limbs paralyzed by upper motor neuron disorders such as spinal cord injury and stroke.

As the functions to be implemented by BIONs become more demanding, the prosthetic system will need to include a growing armamentarium of sensors to detect voluntary command signals and to provide sensory feedback to regulate neuromuscular stimulation. Furthermore, these sensors and actuators need to be readily combinable into custom configurations to deal with the inherent heterogeneity of patients with diverse physiognomies and lifestyles suffering from wide ranges of traumatic and neurological deficits. Rather than designing and implanting a separate set of sensor implants, we decided to reuse the existing resources in BIONs that already need to be implanted for stimulation. This can significantly simplify the design and deployment of the whole prosthetic system. In this paper, we develop and validate techniques to use the microcoil in each BION implant as a magnetic sensor and to integrate information from multiple such magnetic sensors to track the position of limb segments in extrapersonal space.

The BION implant consists of an electronic subassembly with an integrated circuit chip surrounded by a hermetically sealed glass capsule with external electrodes. As illustrated in Fig. 1, the current electronic subassembly is being redesigned to accommodate additional off-chip components such as a MEMS accelerometer [2]. The cylindrical coil around a hollow ferrite core is the antenna of the implant. The coil is connected to the input pads of an ASIC through a ceramic hybrid substrate. In normal operation, it receives power and command data from a frequency-modulated RF magnetic field generated in an external coil worn in the vicinity of the implants. The strength of the received signal depends on the relative distance and orientation between the external and internal coil. The external coil can be turned off briefly while one or more other external coils in known positions are used to create a magnetic field for the implant coil to detect. The measured field strength will be sent by reverse telemetry to an external controller that will compute the position and orientation of the implant with respect to one or more such external reference coils.

The antenna of the BION implant was not designed as a magnetic sensor. The original design focused on maximizing energy transfer with the constraint of capsule shape and size. The multilayer cylindrical coil with hollow ferrite presents properties significantly different from those of an ideal thin-ring coil, whose response can be described easily and accurately with simple mathematic models. To reuse the antenna as a magnetic sensor,

Manuscript received May 29, 2006; revised October 23, 2006; accepted December 6, 2006. This work was supported in part by the National Science Foundation (NSF) Engineering Research Center for Biomimetic MicroElectronic Systems and in part by the Alfred Mann Institute for Biomedical Engineering.

W. Tan was with the A. E. Mann Institute and the Department of Biomedical Engineering, University of Southern California, Los Angeles, CA 90089 USA. He is now with the RBC Product Development Inc., Lenaxa, KS 66215 USA (e-mail: wtan@rbccorp.com).

G. E. Loeb is with the A. E. Mann Institute and the Biomedical Department, University of Southern California, CA 90089 USA (e-mail: gloeb@usc.edu).

Digital Object Identifier 10.1109/TNSRE.2007.897028

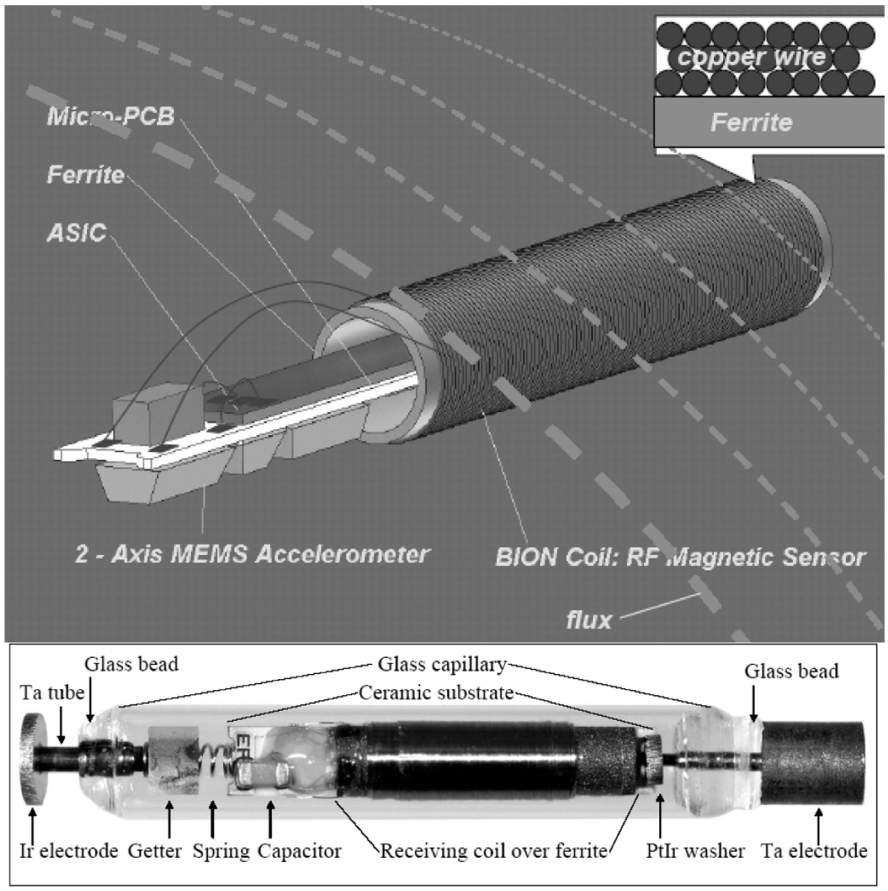

Fig. 1. Top: BION electronic subassembly redesigned for sensors. Multiple microsensors have been developed for posture sensing while keeping the device injectable. Bottom: Current design of BION1 implants for stimulation only, including hermetic glass capsule and electrodes.

a customized model has to be built to predict the response of the BION coil.

II. Properties of Individual Magnetic Emitters and Detectors

A. Idealized Model for Small, Thin Rings

As shown in Fig. 2, if we use ring coils driven by alternating current $\vec{I}$, in free space, the magnetic flux density $\vec{B}$ at point $P(R_0, \theta, \phi)$ defined in 3-D spherical coordinates can be derived from Maxwell's equations as $\vec{B} = \nabla \times \vec{A}$. If we define unit vectors $\mathrm{a_r}$ and a_θ, as shown in Fig. 2, we can determine the magnetic flux density $\vec{B}$ when the diameter of the transmitter is very small compared with the distance r [3]

$$\vec{B} = \frac{\mu_o M}{4\pi R_0^3}(2\cos\theta\vec{a}_r + \sin\theta\vec{a}_\theta) \tag{1}$$

where $M = I\pi\rho^2 a_z$. The induced voltage on an air-core ring coil when it has an angle χ with the $\vec{B}$ vector is proportional to the cosine projection of $\vec{B}$ on the coil axis. Therefore

$$V_{\text{induced}} = k|\vec{B}|\cos\chi \tag{2}$$

k is a constant for a given transmitting coil and a receiving air-core ring coil. This principle has been used by many magnetic sensing schemes [10], [11].

B. Antenna Properties of the BION Coil

The previous model is based on two major assumptions. First, the distance from the sensing coil is relatively large compared with the size of the transmitting coil. Second, both the transmitting coil and the sensing coil are air-core thin rings. As noted above, the antenna of the BION implant is long and cylindrical and wound over a ferrite core to achieve optimal power efficiency within the constraints of the injectable form factor. These result in properties that are not ideal for a magnetic sensor and violate the two aforementioned assumptions. To achieve sufficient field strength over a space many times larger than the transmission coil, the sensing system requires powerful transmitting coils that tend to have substantial thickness, which violates the small, thin ring assumption for the transmitting coil. All these challenges require further investigation focusing on the particular magnetic properties of the BION ferrite coil.

The structure in Fig. 1 illustrates the sources of nonideal effects. The coil is wound with four-layers of copper wire. The final turns of the coil are adjusted so that its inductance and interwinding capacitance achieves a resonant frequency that matches the center frequency of the transmitter, which is 480 kHz. Thus

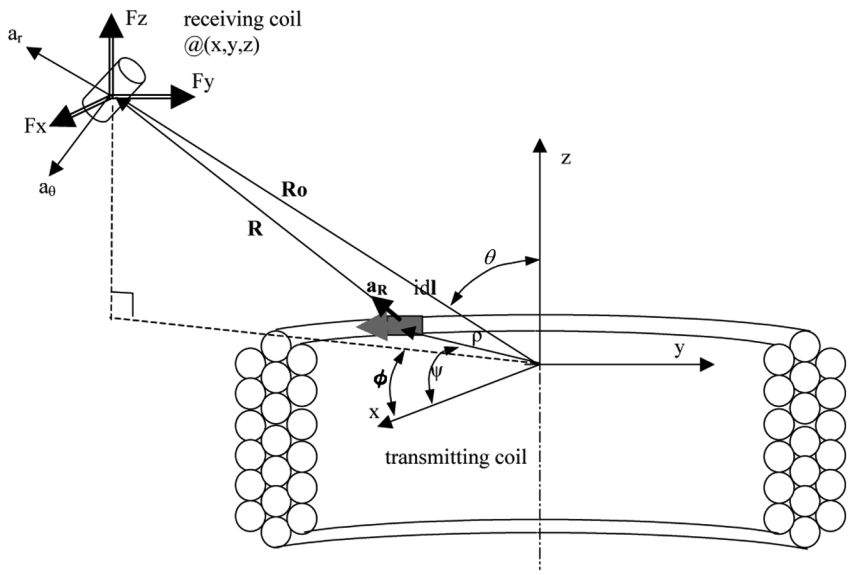

Fig. 2. Magnetic field sensing. A transmitting coil powered with alternating current generates magnetic field that can induce voltage in a receiving coil. Amplitude of the induced voltage is a function of the relative position and orientation between the transmitting coil and receiving coil.

the top layer of the windings is often shorter on one end than the other end after fabrication. Also the margins left at the ends of the ferrite core cannot be guaranteed to be exactly equal. In addition, the ends of the wire are terminated on the same end of the cylinder where they are soldered to the ceramic substrate. All of these factors tend to make the coil longitudinally asymmetrical in its electromagnetic properties. The consequences of these asymmetries are evident in the observation that the induced voltages in the coil change magnitude if the BION receiving coil is flipped by 180°. Moreover, the ferrite material significantly distorts the flux lines in its vicinity, making the voltage deviate from the simple, idealized analytical model.

These electromagnetic effects are difficult to model with analytical equations. Finite element analysis is inappropriate because it is not suitable to be embedded into an algorithm that must actually solve the inverse problem (i.e., determining position and orientation from measured field strength). A more feasible solution is to model these effects according to experimental data, and to adjust the measured sensor signals with function approximation or numerical map. The fitted nonlinear functions can then be used as a correction to improve accuracy. The corrected map from position and orientation to induced voltage then replaces the role of (1) in the solution searching process.

In order to understand and model the various nonideal effects, we isolated each effect and established corresponding models. The first step was to model the response of a BION coil rotating with respect to a fixed magnetic field. The previous paragraph assumes a thin ring with air core, which can be modeled as a simple cosine projection. The actual response of a BION coil is different even though it follows the same trend. Fig. 3 illustrates the induced voltage of the BION coil rotating for 360°. We define the end without wire-bonding as the head of the cylindrical BION coil. When the head of the BION coil is aligned with flux, we define the phase of the induced voltage as positive. We measured the induced voltage as a function of rotation with respect to this reference alignment. The 0° orientation produced $+212$ mV while the $180°(\pi)$ orientation produced -374 mV. For convenience we call the 0° orientation the "low end" and the 180° orientation the "high end." The second effect is that the null orientation is not at 90°, where the BION coil is perpendicular with the flux and the cosine rule for an ideal coil predicts a null. The actual null orientation is displaed from $90°(\pi/2)$ by angle δ.

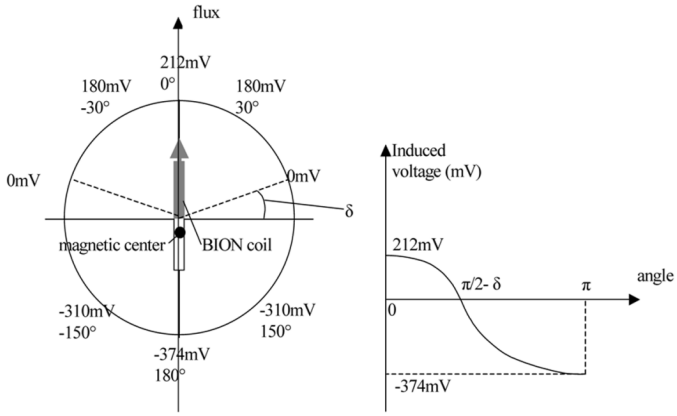

Fig. 3. Axially asymmetric property of the BION Sensing Coil. BION coil wound around a ferrite core presents nonideal magnetic properties due to imperfections in coil fabrication.

Generally, the ferrite material strengthens the flux density inside the coil. However, this effect is not linear with respect to field strength. Further experiments revealed that the amount of deviation from a cosine function as illustrated in Fig. 3 changes with distance from the transmitting coil. To model this effect, we define a scaling parameter μ, which is

$$\mu = \frac{|V_l|}{|V_h|}. \tag{3}$$

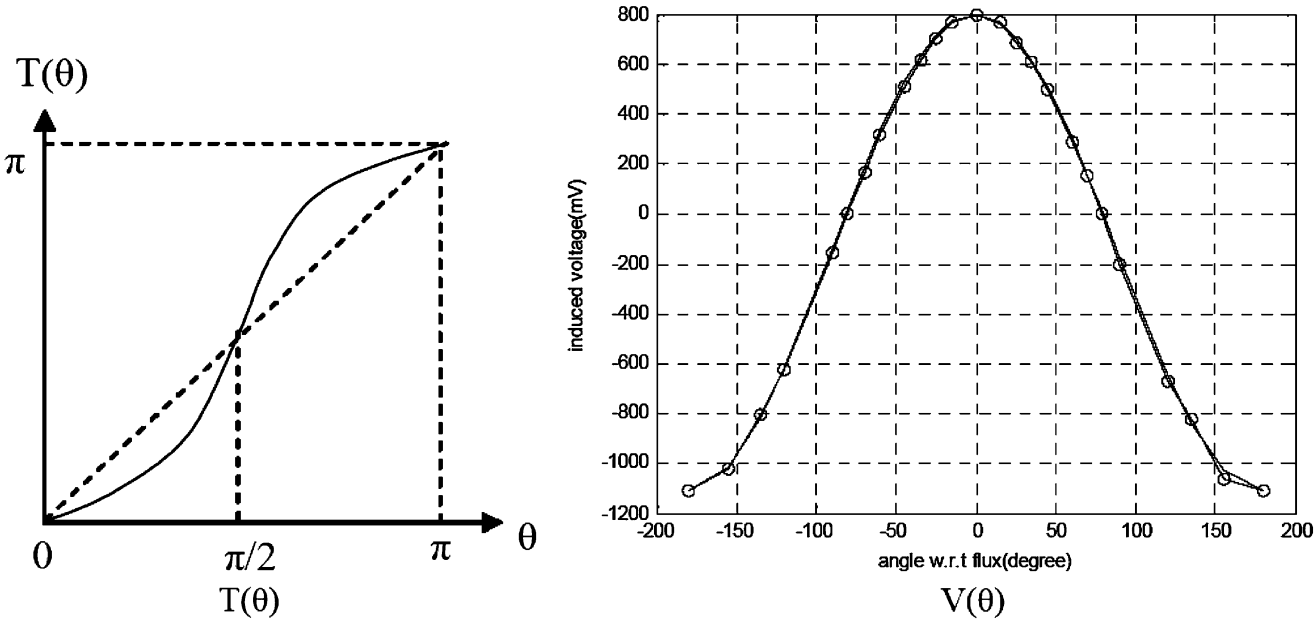

Fig. 4. Left: Shape of the correction function $\mathrm{T}(\theta)$ for rotation of the BION receiver coil with respect to the magnetic field. Right: Experimental data (circles) over 360° rotation and predicted $\mathrm{V}(\theta)$ from (5). Improved model describes accurately the coil property in real world.

V_h and V_l are high end and low end induced voltage, respectively. More extensive experiments revealed that the parameter μ is a function of V_h while almost independent of position in the toroidally curved flux field around the transmitting coil. A set of data was collected at different V_h and used to fit a polynomial function $\mu = f(V_h)$.

After the scaling parameter is modeled, a warped cosine function is used to model the 360° response property

$$V(\theta) = \frac{V_h + V_l}{2} + \frac{V_l - V_h}{2}\cos[T(\theta)\theta]. \tag{4}$$

The nonlinear functions $\mathrm{T}(\theta)$ is used to warp the cosine shape and fit the null orientation. In our application, we empirically choose $T(\theta) = a\theta + b\sin(\theta)$. a and b are tunable parameters

$$V(\theta) = \frac{(1-\mu)V_h}{2} - \frac{(1+\mu)V_h}{2}\cos[a\theta + b\sin(\theta)]. \tag{5}$$

By using an optimization program, the parameter a and b can be found such that

$$a, b \to \min \sum_i \{V_i(\theta) - V_{mi}(\theta)\}^2. \tag{6}$$

$V_i(\theta)$ is the ith computed voltage at angle θ in (4). V_{mi} is the ith measured voltage at angle θ. The fitted function for one BION coil is shown in Fig. 4, superimposed on the data points (circles) obtained experimentally.

At least some of the departures from an "ideal" receiving antenna arise from the asymmetries inherent in winding and terminating the four-layer coil (Fig. 1). Most of the effective interwinding capacitance that gives the coil its self-resonance arises from the turns that are physically close to each other but electrically distant in winding order so as to experience the largest potential differences between them. We have demonstrated that the required resonant frequency of 480 kHz can be obtained with a three-layer coil that has a slightly higher number of total turns than its four-layer equivalent. This inherently more symmetrical coil should reduce the importance of the corrective terms related to asymmetry (see above) that must be extracted from empirical calibration curves.

C. Emission Properties of Large Transmitter Coils

Another important nonideality is the magnetic field generated by the transmitter. When a transmitting coil is relatively large compared with the detecting range, and when the coil shape is different from an ideal thin ring, the magnetic field computed with (1) does not agree well with the experimental measurements.

The first step to improve the modeling of a large transmitting coil is to avoid the simplification used in deriving (1). The approach derives a mathematical description of the magnetic coupling between the two coils in Fig. 2 from basic magnetic principles. As shown in Fig. 2, the large cylindrical coil can be considered as a linear combination of current loops, each of which is composed of infinitely short, straight current segments. The effect of each tiny current segment can be described with Biot–Savart's Law

$$d\vec{H} = \frac{Id\vec{l}\times\vec{R}}{4\pi R^3} = \frac{I}{4\pi R^3}\begin{vmatrix} \vec{a}_x & \vec{a}_y & \vec{a}_z \\ dl_x & dl_y & dl_z \\ R_x & R_y & R_z \end{vmatrix} \tag{7}$$

$d\vec{H}$ is the flux at (x, y, z) generated by the tiny current segment. $\vec{R} = [R_x, R_y, R_z]$ is the vector pointing from the current segment to point (x, y, z). $d\vec{l} = [dl_x, dl_y, dl_z]$ is an infinitely short

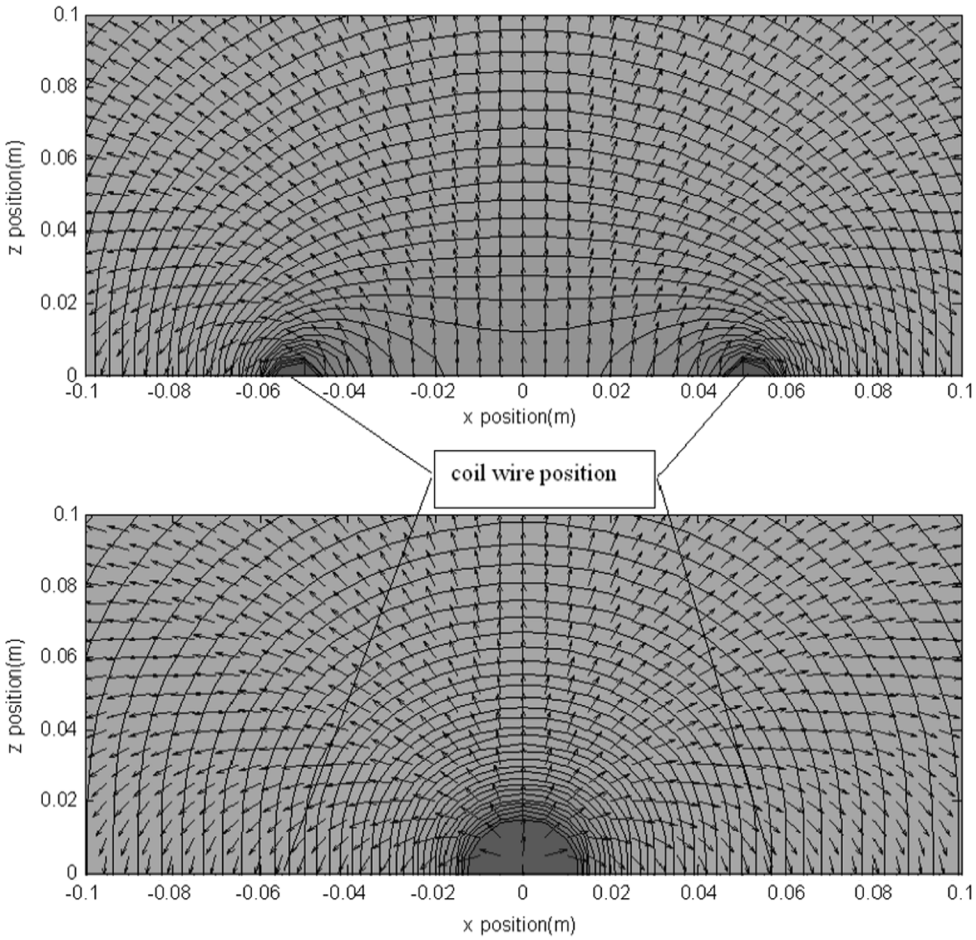

Fig. 5. Magnetic flux lines and field vectors predicted by (1) (bottom) and (7) (top) for the coil illustrated in the insert diagram.

piece of wire. $I$is the current flowing through this wire. Integrating $d\vec{H}$ on the whole transmitting coil by 360° yields the flux at point (x, y, z) caused by one turn of the coil.

R_o and ϕ are defined in Fig. 2. F_x. F_y and F_z are nonlinear functions. The magnetic field can be integrated and decomposed into three orthogonal directions: x, y, and z. Here, we do not assume $\rho \ll R_o$ and we do not simplify (8), shown at the bottom of the page, into the form in (1). Instead a numerical integration can be done on a 2-D matrix of R_o and θ with ϕ assumed as 0. We, therefore, get a function $F_i(R_o, \theta, 0)$ where $i = y$ and z. Then an extra step of rotation transform generates $F_i(R_o, \theta, \phi)$ where $i = x, y$, and z. The effect of the whole coil with many turns can be computed as the linear combination of each turn of the coil at different positions.

Numerical integration of (8) is too computationally intensive to be performed in real-time. It is possible, however, to compute offline $F_i(R_o, \theta, 0)$ where $i = y$ and z and save it as a 2-D data matrix. The real-time computation can be accelerated by using 2-D interpolation based on the saved data. Fig. 5 shows the flux on a 2-D axial plane on one side of a $\phi = 11$ cm cylindrical coil. The position of the plane is illustrated in 3-D in Fig. 6. The difference between top and bottom frames in Fig. 5 shows the

$$\begin{aligned}\vec{H} &= \oint_{\psi} d\vec{H} \\ &= \frac{I\rho}{4\pi}\int_0^{2\pi} \frac{z\cos\psi\vec{a}_x + z\sin\psi\vec{a}_y + [\rho - (y\sin\psi + x\cos\psi)]\vec{a}_z}{[(x-\rho\cos\psi)^2 + (y-\rho\sin\psi)^2 + z^2]^{\frac{3}{2}}} d\psi \\ &= \frac{I\rho}{4\pi}[F_x(R_o,\theta,\phi)\vec{a}_x + F_y(R_o,\theta,\phi)\vec{a}_y + F_z(R_o,\theta,\phi)\vec{a}_z] \end{aligned} \quad (8)$$

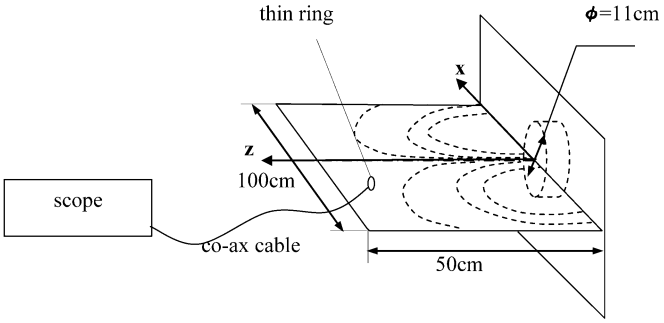

Fig. 6. Experiment setup for calibrating the magnetic field generated by a transmitting coil. Calibration data points can be used to create a compensation function that improves the accuracy of the transmitting coil model.

effect of simplification. The effect is more obvious for regions near the transmitting coil, which is usually a part of the working range of our sensing system when transmitting coils are installed on an armrest. The magnitudes are similar but the directions shift substantially.

Equation (8) is a more accurate model of a large coil than (1), especially for near field. However, mechanical imperfection and the thick cylindrical shape still cause the generated field deviate from (8). To solve this problem, which is hard to model analytically, thin plate splines are used to model the residual error left by (8).

D. Thin Plate Splines to Warp the Transmitted Field

One of the basic problems of 2-D interpolation is to find a smooth surface that interpolates a finite set of N points (x_1, y_1):$z_1, (x_2, y_2) : z_2, \ldots, (x_n, y_n) : z_n$, in which $(x_n, y_n) : z_n$ represents a point with a value of z_n at a 2-D position defined by (x_n, y_n). The problem is usually referred as a surface reconstruction problem. In reality, the data points collected from experiments often do not form an orthogonal mesh due to nonlinear resolution of measurement or limitations of experimental equipment or design. When the mesh is irregular, the data are said to be "scattered."

There are many ways to solve the surface reconstruction problem with scattered data [12]–[14]. Methods based on radial basis functions have the significant advantage that they do not require any information about the connectivity of the scattered data points. In addition, the radial interpolants are invariant to translations and rotations. One such method is the thin plate spline, which has been widely used in applications for interpolation [12].

The surface spline function is used to define a smooth surface such as formed by a steel plate that deforms in bending only. It has mostly been used to solve the function reconstruction problem. A function $\phi(\mathrm{r}_b)$ with a variable r_b is referred to as a radial function

$r_b = \sqrt{(x - x_b)^2 + (y - y_b)^2}$ is the Euclidean distance between the point (x, y) and (x_b, y_b). Therefore, $\phi(r_b)$ is radially symmetric around (x, y). The point (x_b, y_b) is the *center* of radial function. A surface function can be constructed as linear combination of radial functions at different centers

$$f(x) = a_0 + a_1 x + a_2 y + \sum_{b=3}^{n+2} a_b \phi(\sqrt{(x - x_b)^2 + (y - y_b)^2}) \quad (9)$$

where $a_b (b = 1 \sim n_c)$ are unknown coefficients. One of the requirements for the construction of this interpolating surface is the minimization of the energy function

$$E(f) = \iint_{R^2} \left(\frac{\partial^2 f}{\partial x_b^2}\right)^2 + \left(\frac{\partial^2 f}{\partial x_b \partial y_b}\right)^2 + \left(\frac{\partial^2 f}{\partial y_b^2}\right)^2 dx_b dy_b. \quad (10)$$

$E(f)$ indicates the energy stored in elastic deformation of the plate described with f(x). Minimizing $E(f)$ produces a smooth surface with minimal elastic deformation. The function

$$\phi(x) = -r_b^2 \log\left(r_b^2\right) \quad (11)$$

satisfies the energy minimization requirement. $\phi(x)$ satisfies the equation

$$\Delta^2 \phi = \left(\frac{\partial^2}{\partial x^2} + \frac{\partial^2}{\partial y^2}\right)^2 \phi \propto \delta_{(0,0)}. \quad (12)$$

That is, $\phi(x)$ is a fundamental solution of the biharmonic equation $\Delta^2 \phi = 0$. Substitute $\phi(x)$ into f(x) yields the complete form of a surface function

$$f(\vec{x}) = a_0 + a_1 x + a_2 y + \sum_{b=3}^{n+2} a_b ||\vec{x} - \vec{c}_b||^2 \times \log\left(||\vec{x} - \vec{c}_b||^2\right) \quad (13)$$

in which $\vec{c}_b = (x_b, y_b)$ is the bth radial function center and also the position of a scattered data point. The function has been used to describe the shape of a thin steel plate constrained by scattered points at (x_b, y_b) and is therefore called thin plate splines. In our application, we can use the function to interpolate scattered data points collected through calibration. The interpolation task is to identify the coefficients in f(x).

Assume $P_1 = (x_1, y_1), P_2 = (x_2, y_2), \ldots, P_n = (x_n, y_n)$ are n points in the spline function space. $r_{\mathrm{ij}} = |P_i - P_j|$. Because the surface values at all these data points are linear combinations

of radial functions centered at these data points, the relation can be written in matrix form. Define the matrices

$$K = \begin{bmatrix} 0 & \phi(r_{12}) & \cdots & \phi(r_{1n}) \\ \phi(r_{21}) & 0 & \cdots & \phi(r_{2n}) \\ \cdots & \cdots & 0 & \cdots \\ \phi(r_{n1}) & \phi(r_{n2}) & \cdots & 0 \end{bmatrix}_{n\times n}$$

$$P = \begin{bmatrix} 1 & x_1 & y_1 \\ 1 & x_2 & y_2 \\ \cdots & \cdots & \cdots \\ 1 & x_n & y_n \end{bmatrix}_{3\times n}$$

$$L = \begin{bmatrix} K & P \\ P^T & O \end{bmatrix}_{(n+3)}. \tag{14}$$

And $\vec{V} = (v_1, v_2, \ldots, v_n)$ is a n-vector formed by the surface values at data points $1 \sim n$. A zero-padded $n+3$ vector Y is built upon $\mathrm{V} : \vec{Y} = (\vec{V}|000)^T$. Define the spline coefficient vector as $\vec{W} = (w_1, w_2, \ldots, w_{n+3})$. Therefore, $\vec{Y} = L\vec{W}$. The coefficients can be solved by

$$\vec{W} = L^{-1}Y. \tag{15}$$

Reference [15] describes techniques that can compute the inverse of L. The vector $\vec{W}$ can be saved for real-time computation.

E. Calibration Procedure for Thin-Plate Spline

With the 2-D data fitting method, the errors in magnetic sensing can be modeled and calculated by a thin plate spline function. Experiments demonstrate that a transmitting coil can be easily fabricated with proper tools to be axially symmetric. All the error correction can be, therefore, simplified as direction and amplitude warping in a 2-D axial plane.

The first step is to collect the necessary data points on the 2-D plane over the detecting range. Because the thin plate spline is for scattered data, there is no need to form a strict grid. The data includes direction and strength of the magnetic field at the data point defined by coordinates. The theoretical values computed with (1) or (8) are then compared with these experimental data and generate angle and amplitude errors at each point. After that, by reconstructing a smooth interpolation function on the errors upon the scattered data points, we can approximate these errors with the function and cancel these errors based on optimization algorithms.

A sensing coil close to a thin ring can be used to calibrate the magnetic field generated by a transmitting coil. Experiments were done with a two-layer coil with 18 turns of AWG13 Litz wire on a form with 11 cm diameter.

Because the field generated by a transmitting coil is axially symmetric, only points on half of the plane are collected. The process includes four steps.

1) Detect actual flux direction with a small thin ring coil. In this step, we used a 1.5-cm-diameter thin coil wound with 15 turns of AWG 35 wire. When the coil is aligned orthogonal with the flux, the induced voltage is zero. Because the coil is air-core, the response over 360° is almost identical with the cosine law. Therefore, the null orientation is exactly at 90°. With this method 125 points were measured on the plane.
2) Compute the theoretical flux direction at the 125 points measured in step 1 with (1) or (8). Measure their angles

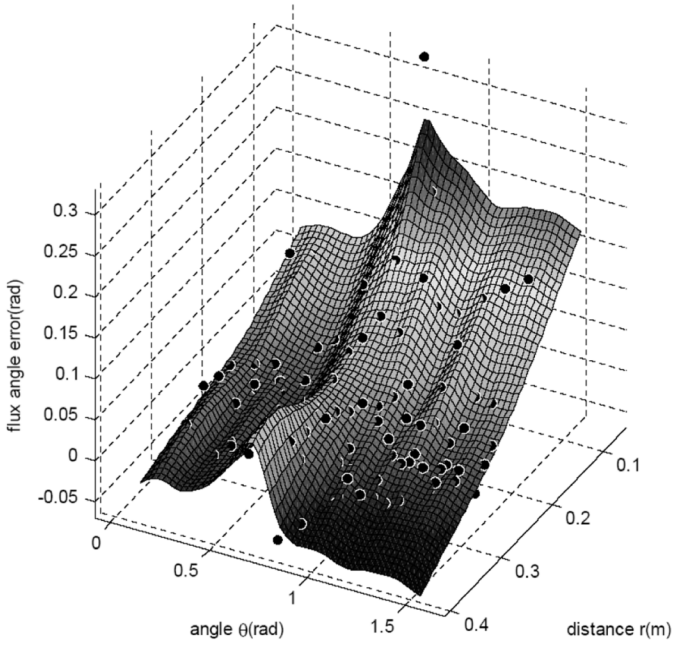

Fig. 7. Thin-plate spline function used to warp the flux direction and reduce error.

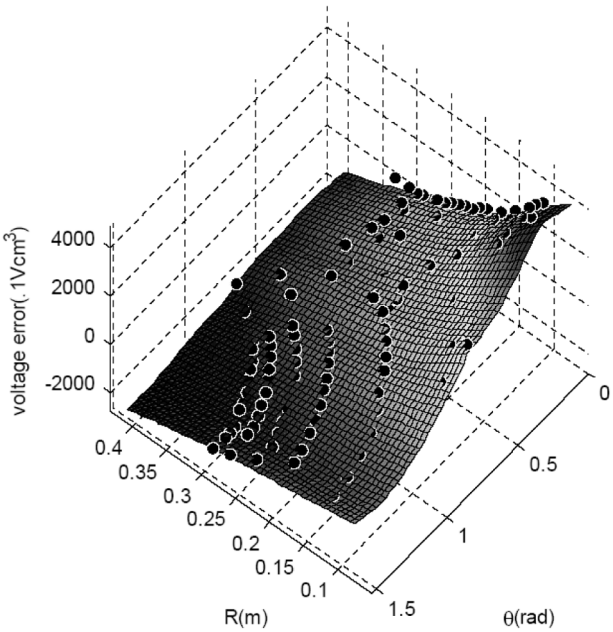

Fig. 8. Amplitude error and thin plate spline function of 125 points. Error depending on 6-D position and orientation variables can be isolated with 2-D functions for direction and amplitude, which are easy to implement in algorithms error.

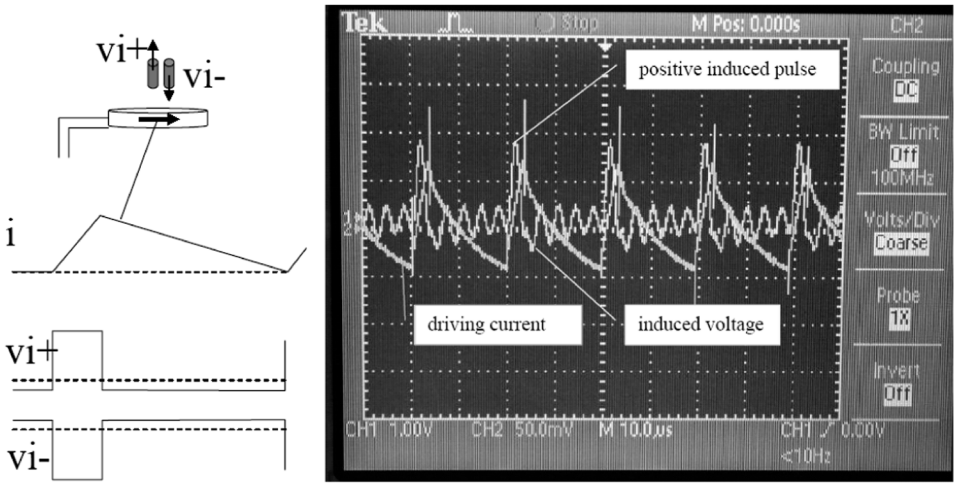

Fig. 9. Excitation method to measure phase as well as magnitude. Sawtooth current pulses (rather than a continuous sinusoidal waveform) in the transmitter coil induce asymmetrical responses in the receiver coil. By detecting both the sign and magnitude of the largest induced voltage, the orientation of the BION implant can be determined unambiguously.

to the axis of the transmitting coil. Subtract the measured angles from the theoretical angles to generate error angles.

3) Construct a thin plate spline with the method mentioned in last section to approximate the error angles.
4) Use the solved thin plate spline function as a warping function to correct the computed flux directions to match the measured flux directions.
5) Convert the 2-D warping into 3-D space.

With the spline function constructed in Fig. 7, direction warping can also be done in real-time with the spline function.

After warping of flux directions, the next step is to correct the amplitude. The error of the induced voltage amplitude is caused by nonideal shape of both the transmitting coil and the receiving coil. Therefore, a calibration is for a given transmitter and receiver pair that will be used in position and orientation sensing. In our case, it is a transmitting coil whose flux directions are corrected above, and a BION sensing coil with the structure, as shown in Fig. 1. Similar steps are followed to calibrate the amplitude errors by aligning the BION coil into the "high end" direction. Because the induced voltage drops drastically with respect to distance, the error here is scaled by $(1/r^3)$ to avoid large computation error. The "high end" amplitude errors are calibrated and interpolated with a thin plate spline function, as shown in Fig. 8.

F. Generation of Pulsed Magnetic Fields

Because a given BION implant is free to move through the null orientation of the magnetic field that it is sensing, it would be useful to be able to sense the phase as well as the magnitude of the magnetic field. If the transmitted field is sinusoidal, the sensor has no reference signal by which to judge phase.

This problem can be solved with a pulsed current generator such as can be produced by rapidly discharging a capacitor in a relaxation oscillator. The induced voltage on the BION sensing coil is negatively proportional to the time derivative of the flux and, therefore, the derivative of the current driving the external coil. If the driving current is an asymmetrical "sawtooth," then the faster first (positive) phase will generate a larger magnitude voltage in the sensing coil than the slower second (negative). The sign of the larger peak tells which direction the sensing coil is oriented with respect to the transmitting coil (Fig. 9 left). In reality because the BION sensing coil is tuned to resonate at 480 kHz, the step voltage actually will be a smooth pulse with harmonic ripples, as measured experimentally (Fig. 9 right). Nevertheless, the peak of the pulse will indicate both the sign and amplitude of the induced voltage.

III. Integration of Multiple Sensors

A reference $x0$-$y0$-$z0$ coordinate is defined, as shown in Fig. 2. The position and orientation of the implanted BIONs and, therefore, the posture of the limb can be described with respect to this reference. Equation (8) can be abstracted here as

$$V_{Tj\_Si} = F(x, y, z, \alpha, \beta, \gamma) \tag{16}$$

where V_{Tj_Si} is the induced voltage on ith BION sensing coil by jth transmitting coil on the wheelchair. α, β, and γ are Euler angles with respect to a reference frame. For a given set of position (x, y, z) and orientation, the voltage sensed by the BION sensing coil can be computed according to F. To use small coils as posture sensors, we need to solve an inverse problem: given the voltages $V_{Ti\_Sj}(i = 1 \sim n, j = 1 \sim m)$ induced on sensing coil j by transmitting coil i, solve the position and orientation.

The task of sensing the upper arm posture provides a general example because it has 6 degree-of-freedom (DOF). It is also particularly clinically relevant because most quadriplegic patients retain substantial voluntary control of shoulder rotation and translation, which can be detected to provide command signals for FES of more distal, paralyzed joints. The upper arm posture can be described as the location of the center of rotation of the shoulder joint (xs, ys, zs) plus the angular orientation of the upper arm (α, β, γ). It should be noted that this coordinate frame is with respect to the wheelchair in which the patient is seated, not with respect to the trunk that forms the base of the

shoulder motion. The trunk is likely to have some active or passive mobility within the wheelchair. If the control system needs to know the relative posture of the arm and shoulder with respect to the trunk, additional sensors will have to be placed in or on the trunk to compute its current posture as another input to the overall posture sensing system.

Generally, if we have m transmitting coils that are turned on and off in sequence, and n receiving coils that can sense the voltage induced by each transmitting coil, we denote the measured voltage of the ith receiving coil induced by the jth transmitting coil as VM_{Tj_Si}. The objective is to minimize the function

$$\mathrm{FA} = \sum_{j=1}^{m}\sum_{i=1}^{n}(\mathrm{VM}_{Tj\_Si} - V_{Tj\_Si})^2. \tag{17}$$

FA is an error function indicating the difference between the measured value and the calculated value. If an algorithm finds the proper position and orientation, the calculated V_{Tj_Si} will be equal to VM_{Tj_Si} and FA will be zero. In reality the algorithm may be unable to make FA exactly zero due to noise, measurement error and computation error. Minimization of FA provides a more practical, "least square" solution compared to solving equations with Newton's method. Using the amplitude of FA as a criteria, a searching algorithm seeks a set of position and orientation, which can produce a group of calculated V_{Tj_Si} approaching VM_{Tj_Si}. The problem can be further constrained by *a priori* knowledge. For example, the rotation quaternion should be a unit quaternion, and there are likely to be anatomical constraints on the possible position and orientation.

A. Multiple Magnetic Emitters

It is difficult to provide strict conditions and proof for when the above problem has a unique solution and best sensitivity in the face of noise in the sensors. However, some design guidelines can be derived from our application scenario. As described in (1), the strength of the received signal declines rapidly with distance from the transmitting coils (generally with the distance cubed), so it is advantageous to position the transmitting coils so that they are generally close to but at varying distances from the various sensors implanted in the limb.

Many candidates for FES to reanimate the arm and hand are confined to wheelchairs, e.g., quadriplegia following spinal cord injury. The sensing scheme has a transmitting box that can be installed on the armrest of a wheelchair (Fig. 10). Multiple coils are installed on the box with different positions and orientations. For a single BION sensor, the number of transmitting coils should be higher than five. Increasing the number of transmitting coils adds redundancy and improves accuracy over the work space.

By locating the transmitting coils in the armrest, it is unlikely that large metal objects will come between transmitting and sensing coils. One exception, however, is the transmitting coil that powers the implant, which is designed to be worn on the arm itself. We have demonstrated that the electromagnetic effects of this coil are negligible if this coil is disconnected from its driver circuitry by an electronic switch for the brief intervals during which position measurements are made. Simply powering down the coil is insufficient because it is part of a high-Q tank circuit in the Class E coil-driver. The switch opening can and should be timed to occur when the voltage across the coil passes through zero and energy can be stored in the tuning capacitor, facilitating a rapid and efficient restart [1], [16].

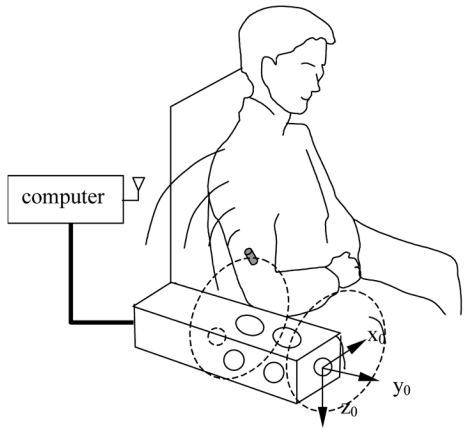

Fig. 10. Posture sensing with BION assembly. Position and orientation of the arm can be sensed wirelessly with BIONs for patient confined in a wheelchair.

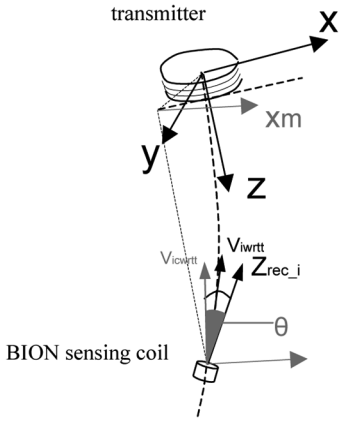

Fig. 11. Converting 2-D warping into 3-D warping. The 2-D calibrated results developed in Figs. 7 and 8 need to rotate to compute the magnetic field at any point in a 3-D space.

The significant benefit of defining the problem as an optimization process is that it naturally handles sensor redundancy. Additional transmitting coils or sensing coils can be added to the system to improve accuracy or robustness of the solution without structural modifications to either the hardware or algorithm. The calibration methods described in Figs. 6–8 apply generally to transmission and sensing coils of a particular design. The empirically determined parameters of these spline functions can be saved for use in real-time computation of limb posture.

The conversion process starts with (16), which gives an uncorrected voltage vector $\vec{V}_{rwrtt} = V_{Tj\_Si}$ with respect to the transmitter coordinates. The voltage vector's amplitude is the amplitude of the induced voltage; the direction is the direction of the flux. Next $\vec{V}_{rwrtt}$ is rotated to the plane on which the sensing coil locates (Fig. 11). The plane is the calibration plane rotated by angle ϕ, which we define as a middle plane for convenience

$$\vec{V}_{iwrtm} = R_m^t(z,\phi)\vec{V}_{iwrtt} = (R_t^m)^T(z,\phi)\vec{V}_{iwrtt}. \tag{18}$$

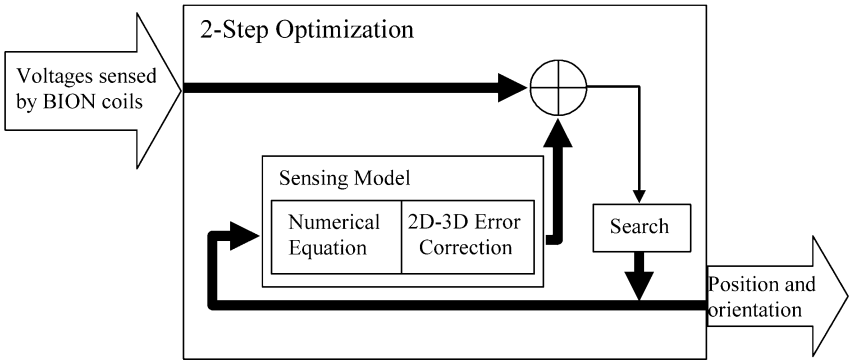

Fig. 12. Algorithm diagram for solving position and orientation with magnetic sensing. Position and orientation of an implanted BION coil are calculated with optimization based on combined magnetic sensors and accelerometers in BION capsule.

On this plane the direction warping is done with the thin plate spline generated offline with the experimental data. The operation is basically a rotation around an axis orthogonal to the middle plane. The final converted voltage vector with respect to the transmitter coordinates can be derived from the inverse rotation matrix of R_m^t

$$\vec{V}_{ciwrtt} = \left(R_m^t\right)^T \vec{V}_{ciwrtm} = \left(R_m^t\right)^T R_{\text{angle}} R_m^t \vec{V}_{iwrtt}. \tag{19}$$

The amplitude is also warped through the similar process.

The final architecture of the algorithm for position and orientation is implemented, as shown in Fig. 12.

The algorithm is actually solving an inverse problem of the sensing model. The above analysis allows us to generate an accurate sensing model that predicts the voltages sensed by a BION coil at a given position and orientation with respect to a transmitting coil assembly. The algorithm starts with a random point within the solution space. The searching process is driven by the error between the output of the model and the measurement. The more accurate the sensing model is, the better the performance of the algorithm. In the first step, a genetic algorithm helps to avoid local minima and brings the search quickly to a region near the accurate solution. However, the genetic algorithm performs poorly on convergence. The second step is a trust region approach [6], [7] for nonlinear minimization, which does not rely on an analytical model for gradient information. The optimization converges to a solution when the least square error between the induced voltages predicted by the model and the measured voltages is within a threshold.

B. Weighted Contribution from Multiple Sensors

One of the special properties of magnetic sensing is high nonlinearity. The sensitivity of a search coil to changes of position and orientation is uneven over the sensing space. More specifically, the sensing coil is maximally sensitive to rotation but minimally sensitive to translation when it is near the null orientation. The null orientation is the direction where the BION coil axis is orthogonal to the flux. At this orientation, the amplitude of F is zero but the derivative $(\partial F/\partial\theta)$ is the largest, where F is the voltage function as shown in (16) and θ is the solid angle illustrated in Fig. 11. This situation can adversely affect the genetic algorithm that is trying to solve the inverse problem. The searching step illustrated in Fig. 12 can be greatly affected by small errors such as in the positioning of the transmitting antennas or sliding motion among the implanted sensors. Because the signals are small near the null orientation, small noise values imply relatively large angular shifts from the correct orientation. Thus, the genetic algorithm may miss a narrow, deep optimal solution and deviate into broader local minima. To reduce these negative effects and make the algorithm more robust, the minimization algorithm in (17) can be modified to weight the signals individually

$$\min \quad FA = \sum_{j=1}^{m}\sum_{i=1}^{n} w_i (VM_{Tj\_Si} - V_{Tj\_Si})^2. \tag{20}$$

When the algorithm detects that the measured voltage is very small, it assumes that the sensing coil is close to null orientation and regards the signal as less trustable. The weight parameter w_i in (20) is, therefore, scaled down. Because of the redundancy in the system, the algorithm can still reach the correct solution quickly even if this assumption is incorrect.

C. Integration With dc-Accelerometer

Magnetic sensing via a single BION antenna will be insensitive to axial rotation no matter how many transmitting coils are used or how they are arranged. The two-axis accelerometer developed for these implants [8] can resolve the sixth DOF. It also provides redundancy when combined with the magnetic sensing system, which could be used to detect, if not resolve, distortions of the magnetic field for which the magnetic sensing algorithm cannot converge on a reasonable solution. For simplicity, we use the two-axis accelerometer only as a static sensor to sense inclination with respect to gravity. For a patient making slow arm movements while confined to a wheelchair, the dynamic acceleration experienced by a BION inside a patient's upper arm is generally less than 0.05 g, which should be negligible compared to the ± 1 g range of gravity acting on the implant. (One exception to this would be impact with an external object, which would produce a large, synchronous signal in the accelerometers of all implants. Such an event would be easy to detect and the algorithm would need to ignore such spurious data.) In the pitch-roll-yaw coordinate frame (Euler angles α, β, and γ), the inclination of a two-axis accelerometer can be computed from sensed gravity. These angles will generally be computable also through the magnetic sensing mechanism, and always if at least two noncolinear sensors are available. This redundancy can be

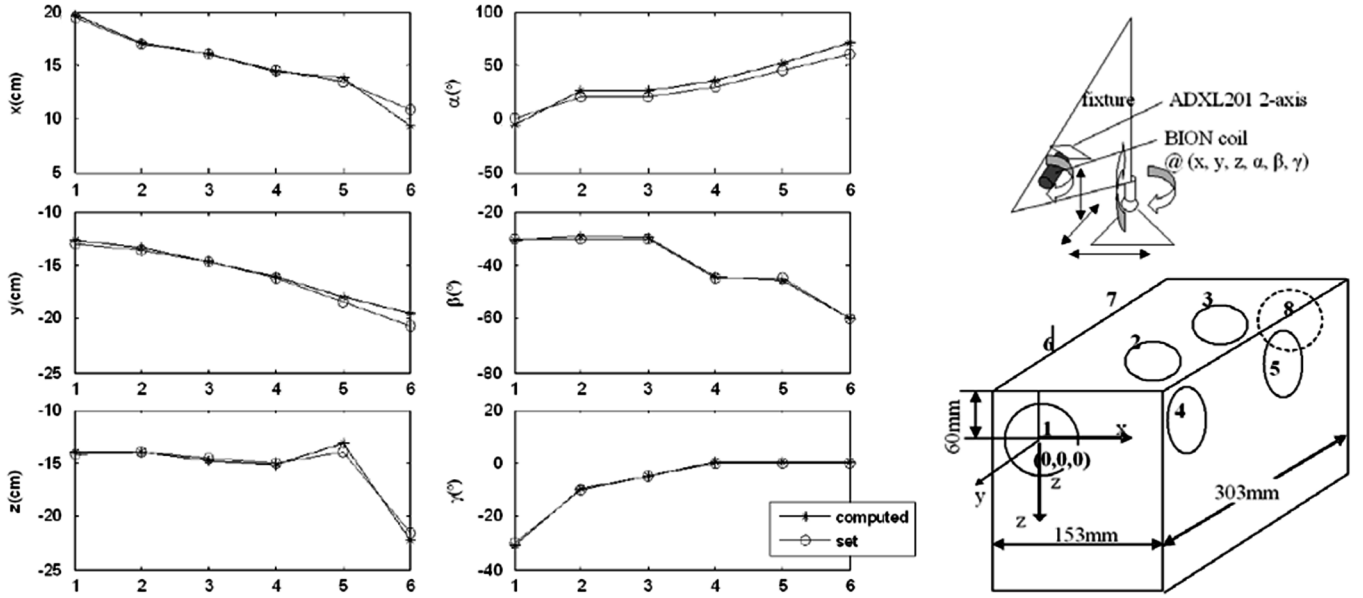

Fig. 13. Experimental results measured with BION coil. An assembly of eight transmitting coils is installed as a reference. A representative trajectory is computed from induced voltages in a BION sensing coil and 2-D gravity signals.

utilized by sensor fusion algorithms such as a Kalman filter to suppress noise and improve robustness.

D. Optimal Estimation of Current Posture

The solution space for determining limb position and orientation from many individually nonlinear sensors is likely to have many local minima. Given sensor noise and calibration errors, there may not be a statistically significant global minimum. Perhaps the most useful constraint will be the previous posture. Natural limb movements tend to be highly constrained by the inertial mass of the limb segments, their linkage through joints with limited DOF, and the limited frequency response and force generating abilities of muscles. Biomechanical constraints such as smooth, incremental motion can be formalized through the use of extended Kalman filtering. This will require, however, that the prosthetic system be initialized in some known starting posture. For example, the hands could be located on a lap tray that the operator would normally use to support the arms when the FES system is not in use. This starting posture need not be accurate, as long as it does not straddle two local minima in the posture solution.

In general, it will be desirable to avoid having closely spaced postures that produce similar sets of signals in the sensors (i.e., local minima in the solution space). This consideration should prove useful in configuring the transmitting coils for a given patient. The position and orientation of the sensing implants could also be chosen on this basis, but these may be highly constrained by considerations related to stimulation of the muscles. It will generally be desirable to use the same implants for stimulation and sensing in order to minimize the total number of implanted devices. Because the best placement for stimulation is usually near the middle of the muscle belly, the implants are likely to shift position within the limb as the muscles contract and relax. A method to correct for this is presented below.

TABLE I
UNITS FOR MAGNETIC PROPERTIES

	X(cm)	Y(cm)	Z(cm)	α(°)	β(°)	γ(°)
1	19.48	13.07	14.2	0	30	30
2	17	13.62	13.9	20	30	10
3	16.02	14.69	14.5	20	30	5
4	14.48	16.25	15	30	45	0
5	13.5	18.43	14	45	45	0
6	10.83	20.65	21.49	60	60	0

Six points of BION implant along a representative arm trajectory are designed for the test. The angles are modified to close values for an easy setup of the fixture. The positions and Euler angles are defined with respect to the x-y-z coordinates in Fig. 13.

IV. EXPERIMENTAL VALIDATION

In order to validate the magnetic sensing scheme presented in Fig. 10, we performed an experiment with the transmitting coils installed at known positions and orientations. After the position and orientation of each BION receiving coil was computed, the posture of the mechanical arm on which they were mounted was described in reference to a 0 frame, with reference to the transmitting coils, as shown in Figs. 10 and 13. All the modeling techniques mentioned above were used as a part of the algorithm outlined in Fig. 12. The calibrated BION coil was installed on an adjustable fixture made of poly-carbonate plastic, which is transparent to the magnetic field and does not present any interference to the measured voltages.

Eight transmitting coils were installed in a box with different orientations and locations (Fig. 13). The coils were arranged such that the size and the shape of box could fit an armrest of a wheelchair. Distributing the coils over the available distance decreases distortion due to mutual inductance among them and increases the likelihood that the sensor will be a region of high field strength. To further reduce interference, an electronic switch opened the circuit to all the other coils when one coil transmitted.

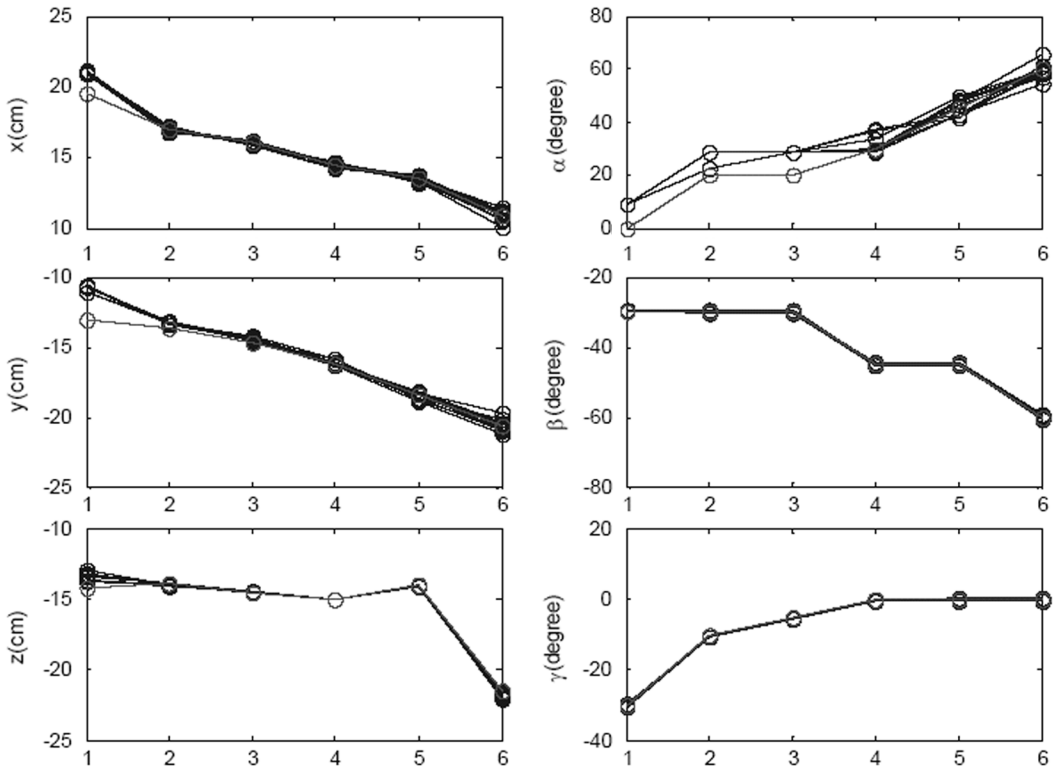

Fig. 14. Monte Carlo simulation on algorithm robustness. Sensing coil voltages and accelerations are simulated with random variables to test the effect of measurement errors on computed postures.

A BION receiving coil was held in a fixture that could be set to calibrated 2-D translation and 3-D rotation. A commercial ADXL201 two-axis accelerometer was installed with the BION coil to provide two-axis acceleration. The MEMS accelerometer developed for the BION is expected to perform similarly. The receiving BION coil was set to a series of positions and orientations mimicking the trajectory of the upper arm in a typical reach and grasp task (values listed in Table I).

The computed points in Fig. 13 are results generated by the sensing system. The set points are defined by the mechanical fixture. The sensing system generally performs well, with angle errors less than 10° and position errors less than 2 cm. Accurate calibration and a well-fitted mathematic model can reduce the model error. The blue bars in the graphs are computed results based on real measurements. The green bars evaluate the performance of the algorithm by assuming the model error is zero. They demonstrate the performance of the two-step algorithm. The first row is the result of the first step (genetic algorithm), which brings the result close to the solution quickly from a group of random points in the workspace. The second row is the result of the trust region approach, which proceeds from the results of the first step and converges to the real values shown in brown bars. The difference of blue and green bars indicates the effect of the sensing model, while the difference between green and brown bars is computation error. In general, the graphs show how much improvement can be made on the sensing model and on the optimization algorithm, respectively.

Experimental tests have been done on several reach-and-grasp trajectories. In a region of 20 cm × 30 cm × 18 cm, the largest errors in these experiments are less than 1 cm and 10°. These results suggest that a single implant equipped for both magnetic field and gravity sensing could provide useful command and/or feedback signals from a single limb segment. In most FES applications, however, there would likely be multiple such implants in a given segment, whose sensor data can be combined to improve accuracy. For example, the forearm would have at least four BIONs to control the antagonist muscle pairs used for wrist flexion/extension and ulnar/radial deviation. Most of the residual error for the single implant mock-up illustrated in Fig. 13 is attributable to the manual calibration, which employed coarsely designed fixtures whose accuracy may be similar to clinical calibration procedures in which the arm will be positioned manually in canonical positions. A computerized calibration system with precise mechanical fixtures should reduce the error considerably.

To investigate the effect of measurement variation, Monte Carlo simulation was done on the above trajectory, assuming an exaggerated standard deviation of 30 mV on each coil. Fig. 14 shows the simulation results. Generally, the position sensing is more robust to sensing errors, while angle alpha is more susceptible to signal variation. These errors need to be considered in the context of the limited accuracy of biological kinesthesia [9], the sensitivity of any control algorithms to such errors, and the acceptability of corrective movements made with visual guidance such as commonly occur in natural tasks.

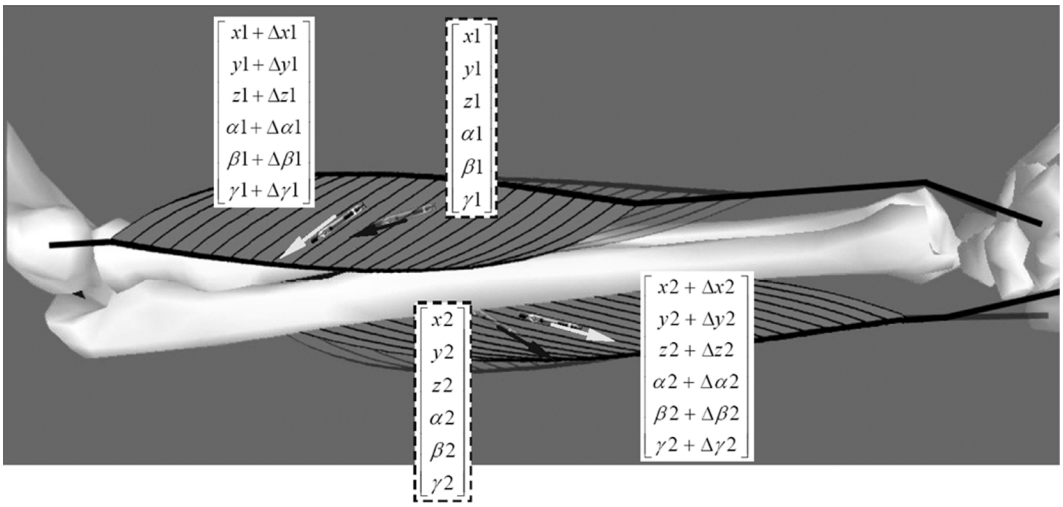

Fig. 15. Arm model considering muscle deformation. Small movement of BION coils caused by muscle deformation can be approximated linearly to the assumed rigid body model of a limb. With the relative movement of BION coils, the arm posture can be more accurately derived from the implanted sensors.

A. Correction for Muscle Deformations

The BION implants are designed to be injected into human muscles. The musculoskeletal system of the arm is actually not a rigid body, as assumed by the above algorithm. BIONs implanted in the muscles will move with respect to each other as the muscles stretch or shorten in concert with motion of the joints that they cross.

Fig. 15 illustrates the situation of BIONs moving with muscles. In this situation, the position and orientation computed for BION coils does not reflect the real posture of the limb segment, which is more correctly defined by the bone. The FES application requires multiple BIONs in each limb segment. A sensor fusion algorithm that can integrate redundant signals and estimate the position and orientation of the bone provides better posture information.

Referring to Fig. 15, let us define the initial position of the wrist as neutral (horizontal; shaded posture). The initial positions (blue arrows) for BION1 and 2 are $[x1, y1, z1, \alpha1, \beta1, \gamma1]$, and $[x2, y2, z2, \alpha2, \beta2, \gamma2]$, respectively. As the arm rotates, the BIONs will move with the muscles and they will also move in the muscles as the muscles deform (yellow arrows). Considering the deviation from their initial positions and orientations, the resulted position and orientation after the rotation can be written as $[x1 + \Delta x1, y1 + \Delta y1, z1 + \Delta z1, \alpha1 + \Delta\alpha1, \beta1 + \Delta\beta1, \gamma1 + \Delta\gamma1]$ and $[x2 + \Delta x2, y2 + \Delta y2, z2 + \Delta z2, \alpha2 + \Delta\alpha2, \beta2 + \Delta\beta2, \gamma2 + \Delta\gamma2]$. The delta values are nonlinear functions of the rotation angles of the arm. Using Euler angles, these values can be expressed as

$$\begin{bmatrix} \Delta x1 \\ \Delta y1 \\ \vdots \\ \Delta\beta2 \\ \Delta\gamma2 \end{bmatrix}_{12\times1} = \begin{bmatrix} f_{x1}(\alpha,\beta,\gamma) \\ f_{y1}(\alpha,\beta,\gamma) \\ \vdots \\ f_{\beta2}(\alpha,\beta,\gamma) \\ f_{\gamma2}(\alpha,\beta,\gamma) \end{bmatrix}_{12\times1}$$

$$\approx \begin{bmatrix} \frac{\partial f_{x1}}{\partial\alpha} & \frac{\partial f_{x1}}{\partial\beta} & \frac{\partial f_{x1}}{\partial\gamma} \\ \frac{\partial f_{y1}}{\partial\alpha} & \frac{\partial f_{y1}}{\partial\beta} & \frac{\partial f_{z1}}{\partial\gamma} \\ \cdots & \cdots & \cdots \\ \frac{\partial f_{\beta2}}{\partial\alpha} & \frac{\partial f_{\beta2}}{\partial\beta} & \frac{\partial f_{\beta2}}{\partial\gamma} \\ \frac{\partial f_{\gamma2}}{\partial\alpha} & \frac{\partial f_{\gamma2}}{\partial\beta} & \frac{\partial f_{\gamma2}}{\partial\gamma} \end{bmatrix}_{12\times3} \begin{bmatrix} \alpha \\ \beta \\ \gamma \end{bmatrix}$$

$$\triangleq \mathbf{F} \begin{bmatrix} \alpha \\ \beta \\ \gamma \end{bmatrix}. \tag{21}$$

We used linear approximation to write the nonlinear functions into the product of a constant matrix $\mathbf{F}$, which is the Jacobian matrix of the nonlinear functions, and a vector that describes the rotation of the bone. If we know the constant matrix $\mathbf{F}$, we will be able to tell how much the BIONs deviate from their initial positions and orientations.

The matrix $\mathbf{F}$ can be measured experimentally from a large group of redundant data. Assuming we sampled n points from different postures, from (22) we can write the following equation:

$$\mathbf{F} = \begin{bmatrix} \Delta x1(2) & \Delta x1(2) & \cdots & \Delta x1(n) \\ \Delta y1(2) & \Delta y1(2) & \cdots & \Delta y1(n) \\ & \vdots & & \\ \Delta\beta2(1) & \Delta\beta2(2) & \cdots & \Delta\beta2(n) \\ \Delta\gamma2(1) & \Delta\gamma2(2) & \cdots & \Delta\gamma2(n) \end{bmatrix}_{12\times n} \times \left(\begin{bmatrix} \alpha(1) & \alpha(2) & \cdots & \alpha(n) \\ \beta(1) & \beta(2) & \cdots & \beta(n) \\ \gamma(1) & \gamma(2) & \cdots & \gamma(n) \end{bmatrix} \right)^{+}_{n\times3}. \tag{22}$$

The $+$ operator is the pseudo-inverse of a matrix, which provides a linear approximation of the matrix $\mathbf{F}$. The quaternion version can also be derived for singular orientations. In application, it is likely that more than two BIONs will be implanted in each arm segment. In this case, the matrix in (22) can simply be expanded in dimension as more BIONs are added.

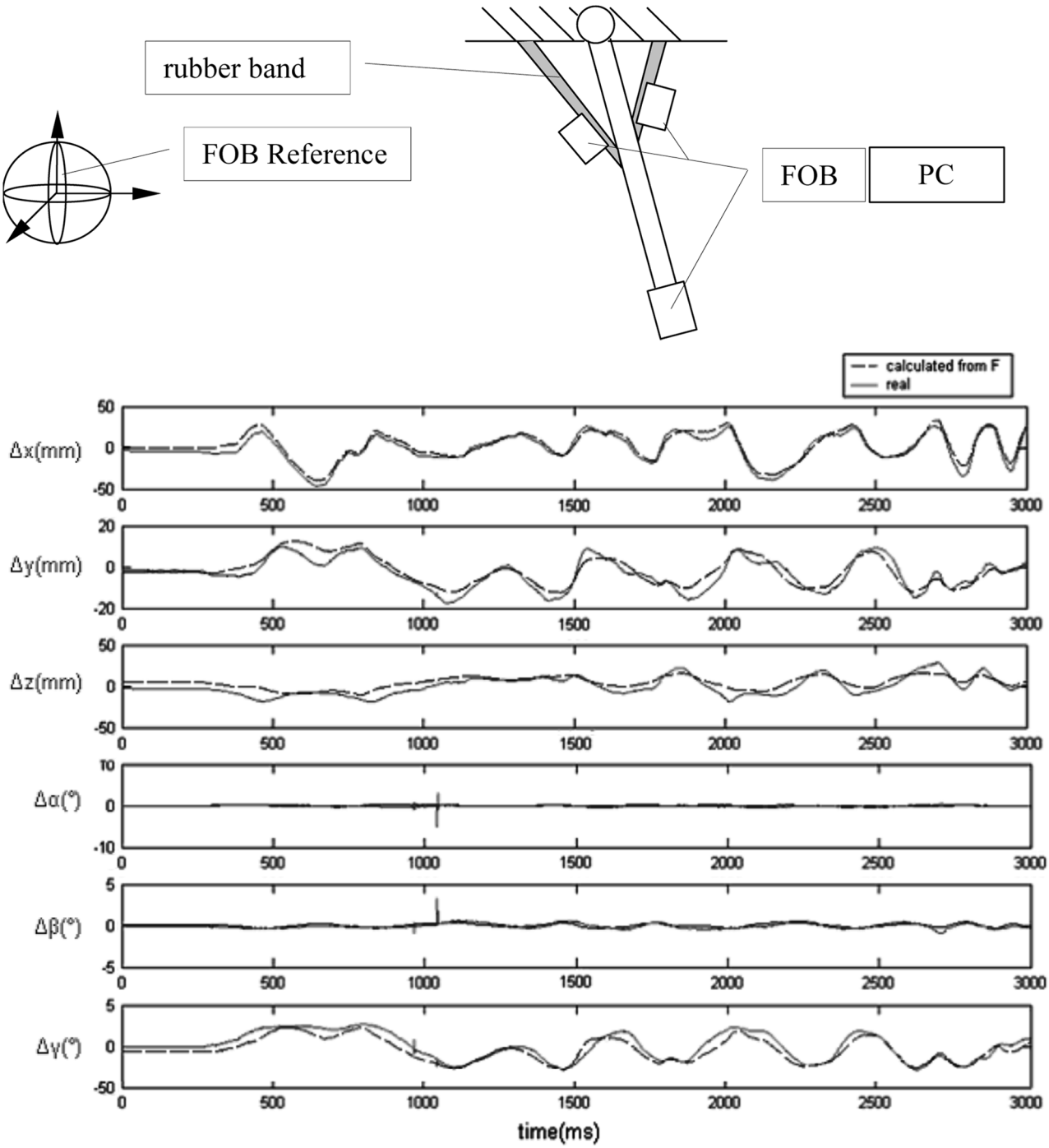

Fig. 16. Experiment of estimating rigid body posture with sensors in elastic material. Small movement caused by the elastic deformation mimics the effect of muscle deformation. Linear approximation method is tested experimentally.

To test the method, a dummy arm was designed to mimic the musculoskeletal system of an upper arm. As shown in Fig. 16, a rigid bar was installed on a fixture to mimic the bone. Two rubber bands were attached to the bar and the fixture to mimic a pair of complementary muscles. Two FOB [10] sensors were installed on the rubber bands. The positions and orientations of the FOB sensors on the rubber band were used to estimate those of the rigid bar. First, the rigid bar was rotated randomly around the orientation space while 3000 samples were collected using the FOB sensing system. With the data we can compute the matrix $\mathbf{F}$ with (24). With $\mathbf{F}$ the delta values of $\Delta x, \Delta y, \Delta z$, $\Delta\alpha, \Delta\beta$, and $\Delta\gamma 1$ can be calculated. The result shows that the calculated position and orientation basically track those of the rigid bar. Actual motion in real muscles will likely be more complex but still mostly deterministic, hence amenable to this general method of correction.

V. Conclusion

We have investigated the feasibility of a posture sensing system based on two sensor modalities that are consistent with the constraints on size and power inherent in the BION implant. A variety of modeling techniques have been proposed and implemented in an inverse problem solving process that can correct for the nonideal behavior of the sensors and combine redundant information to improve accuracy in the face of noise. Experiments have demonstrated promising results for reusing the BION antenna as a magnetic posture sensor.

Combining magnetic field sensing with other modalities having different strengths and weaknesses is likely to improve overall system performance and robustness. We have demonstrated how magnetic sensing can be combined with a two-axis direct current accelerometer developed previously for incorporation into BION implants. It will probably be undesirable to implant and power devices in the hands and fingers to sense posture of the most distal joints, but other BION-compatible sensors have been developed to estimate these from the translational displacement of implants in the forearm muscles that motivate those segments via tendons [17]. The analysis provided here should prioritize and guide further improvements in sensor design, system integration and calibration procedures that will ultimately provide sufficient accuracy for closed-loop control of functional electrical stimulation to reanimate paralyzed limbs.

Acknowledgment

The authors would like to thank Dr. H. Phillips for advice and assistance with the relaxation oscillator and D. Gilliam and E. Ramos for providing transmitting and receiving coils for testing.

References

[1] G. E. Loeb, R. A. Peck, W. H. Moore, and K. Hood, "BION system for distributed neural prosthetic interfaces," *Med. Eng. Phys.*, vol. 23, pp. 9–18, 2001.

[2] G. E. Loeb, W. Tan, N. Sachs, Q. Zou, and E. S. Kim, "A modular approach to sensing limb position in FES patients," presented at the 9th Annu. Meeting Int. Functional Electrical Stimulation Soc., Bournemouth, U.K., 2004.

[3] Q. Zou, W. Tan, E. S. Kim, and G. E. Loeb, "Single-axis and Tri-axis piezoelectric bimorph accelerometer part II: Experimental results and discussion," *J. Microelectromechanical Syst.*, to be published.

[4] W. Tan and G. E. Loeb, "Multimodal injectable sensors for neural prosthetic proprioception," presented at the 1st Int. Conf. Neural Interface Control, Wuhan, China, 2005.

[5] T. F. Coleman and Y. Li, "An interior, trust region approach for nonlinear minimization subject to bounds," *SIAM J. Optimization*, vol. 6, pp. 418–445, 1996.

[6] J. J. MoreG. A. Watson, *The Levenberg-Marquardt Algorithm: Implementation and Theory, Numerical Analysis*. New York: Springer Verlag, 1977, Lecture Notes Mathematics, pp. 105–116.

[7] Q. Zou, W. Tan, E. S. Kim, and G. E. Loeb, "Implantable biaxial piezoresistive accelerometer for sensorimotor control," in *IEEE-EMBS Conf.*, San Francisco, CA, Sep. 1–5, 2004, pp. 4279–4282.

[8] S. C. Gandevia, J. L. Smith, M. Crawford, U. Proske, and J. L. Taylor, "Motor commands contribute to human position sense," *J. Physiol*, vol. 571, no. 3, pp. 703–710, Mar. 2006.

[9] M. N. O. Sadiku, *Elements of Electromagnetics*, 3rd ed. New York: Oxford Univ. Press, 2001.

[10] B. Haim, "System for determining the location and orientation of an invasive medical instrument," U.S. Patent 6 690 963 B2, Feb. 10, 2004.

[11] F. L. Bookstein, "Principal warps: Thin-plate splines and the decomposition of deformations," *IEEE Trans. Pattern Anal. Mach. Intell.*, vol. 11, no. 6, pp. 567–585, Jun. 1989.

[12] A. A. Amini, "Constrained thin-plate spline reconstruction of 2-D deformations from tagged MRI, Proceedings," in *Workshop Biomed. Image Anal.*, 1998, pp. 36–45.

[13] S. Lee, G. Wolberg, and S. Y. Shin, "Scattered data interpolation with multilevel b-splines," *IEEE Trans. Vis. Comput. Graphics*, vol. 3, no. 3, pp. 228–44, Jul.–Sep. 1997.

[14] S. K. Lodha and R. Franke, "Scattered data techniques for surfaces," in *Sci. Visualization Conf.*, 1997, pp. 181–181.

[15] M. J. d. Powell, "On updating the inverse of a KKT matrix," presented at the Int. Conf. Numerical Linear Algebra Optimization, Guilin, China, 2003.

[16] P. R. Troyk, W. Heetderks, M. Schwan, and G. E. Loeb, "Suspended carrier modulation of high-Q transmitters," U.S. Patent 5 697 076, Dec. 9, 1997.

[17] N. A. Sachs and G. E. Loeb, "Development of a BIONic muscle spindle for prosthetic proprioception," *IEEE Trans. Biomed. Eng.*, vol. 54, no. 6, pp. 1031–1041, Jun. 2007.

Wei Tan (M'06) received the diploma in medical instrument from Shanghai Medical Instrument College, Shanghai, China, in 1992, and the M.S. degree in electrical engineering and the Ph.D. degree in biomedical engineering from the University of Southern California, Los Angeles, in 2004 and 2006, respectively.

In 1992, he joined Suzhou Medical Instrument Company as an Electrical Engineer. From 1999 to 2001, he worked as an Electrical Engineer at China Technology Center of General Electric Company. Now he is working with RBC Product Development Corporation, Lexena, KS, as an Electrical Engineer. His research interests include biomedical implants, sensors, and related electronics and algorithms.

Gerald Loeb (M'98) received the B.A. and M.D. degrees from Johns Hopkins University, Baltimore, MD, in 1969 and 1972, respectively.

He did one year of surgical residency at the University of Arizona, Tucson, before joining the Laboratory of Neural Control at the National Institutes of Health (1973–1988). He was Professor of Physiology and Biomedical Engineering at Queen's University, Kingston, ON, Canada (1988–1999) and is now Professor of Biomedical Engineering and Director of the Medical Device Development Facility of the A. E. Mann Institute for Biomedical Engineering, University of Southern California, Los Angeles. He was one of the original developers of the cochlear implant to restore hearing to the deaf and was Chief Scientist for Advanced Bionics Corporation (1994–1999), manufacturers of the Clarion cochlear implant. Most of his current research is directed toward neural prosthetics to reanimate paralyzed muscles and limbs using a new technology that he and his collaborators developed called BIONs. This work is one of the testbeds in the NSF Engineering Research Center on Biomimetic MicroElectronic Systems, for which he is Deputy Director. These clinical applications build on his long-standing basic research into the properties and natural activities of muscles, motoneurons, proprioceptors, and spinal reflexes. He is a holder of 38 issued U.S. patents and author of over 200 scientific papers.

Dr. Loeb is a Fellow of the American Institute of Medical and Biological Engineers.